An improved rainflow algorithm combined with linear criterion for the accurate li-ion battery residual life prediction.

HUANG, J., WANG, S., XU, W., FERNANDEZ, C., FAN, Y. and CHEN, X.

2021

Int. J. Electrochem. Sci., 16 **(2021)** Article ID: 21075, doi: 10.20964/2021.07.29

International Journal of
ELECTROCHEMICAL
SCIENCE
www.electrochemsci.org

An Improved Rainflow Algorithm Combined with Linear Criterion for the Accurate Li-ion Battery Residual Life Prediction

Junhan Huang[1], *Shunli Wang*[1,*], *Wenhua Xu*[1], *Carlos Fernandez*[2], *Yongcun Fan*[1] , *Xianpei Chen*[1]

[1] School of Information Engineering, Southwest University of Science and Technology, Mianyang 621010, China;
[2] School of Pharmacy and Life Sciences, Robert Gordon University, Aberdeen AB10-7GJ, UK.
[*]E-mail: wangshunli@swust.edu.cn

Received: 9 February 2021 / *Accepted:* 3 April 2021 / *Published:* 31 May 2021

Li-ion battery health assessment has been widely used in electric vehicles, unmanned aerial vehicle and other fields. In this paper, a new linear prediction method is proposed. By weakening the sensitivity of the Rainflow algorithm to the peak data, it can be applied to the field of battery, and can accurately count the number of Li-ion battery cycles, and skip the cumbersome link of parameter identification. Then, a linear criterion is proposed based on the idea of proportion, which makes the life prediction of Li-ion battery linear. Under the verification of multiple sets of data, the prediction error of this method is kept within 2.53%. This method has the advantages of high operation efficiency and simple operation, which provides a new idea for battery life prediction in the field of electric vehicles and aerospace.

Keywords: Li-ion battery; state of charge; unscented Kalman filtering; Rainflow; linear prediction criterion

1. INTRODUCTION

Li-ion battery has the advantages of high energy density[1-4], long life, high output power [5] and high-cost performance, which plays an important role in the field of renewable energy[6]. With the new energy industry more and more attention, the use of Li-ion batteries is increasing year by year. At present, the prediction of Li-ion battery cycle life is still a long way from the mature practical online application. The prediction of Li-ion battery cycle life is the core and difficulty of Battery Management System (BMS) [7-9]. Many military electronic devices, such as GPS system and unmanned aerial vehicle (UAV) , rely on Li-ion batteries for portable power supply . The reliability of Li-ion batteries needs to be evaluated to avoid serious consequences of Li-ion battery failure, such as operation damage, performance degradation, and even catastrophic failure. To ensure the reliability of Li-ion batteries in

operation, it is necessary to evaluate the capacity of Li-ion batteries and predict the remaining cycle life [10]. The State of Health (SOH) estimation [11-13] of Li-ion batteries is an important part of BMS. Therefore, accurate and efficient prediction of the remaining life of Li-ion batteries plays an important role in the safety and economic evaluation of equipment.

In the field of Li-ion battery SOH estimation, there are three commonly used methods, the first is battery impedance [14]. Guangzhong et al. mainly used Brownian motion and particle filter methods to estimate the short-term SOH of lithium-ion batteries and the long-term prediction of RUL. The nonlinear drift and scaling parameters in Brownian motion are used to infer the dynamic behavior of lithium-ion battery degradation, the lithium battery capacity degradation model is established, and the particle filter algorithm is used to estimate the parameters in Brownian motion[15].Hu et al. Evaluated the optimized driven moving horizon estimation (MHE) framework in detail through a simplified electrochemical model, and demonstrated the feasibility and performance of accessing the internal battery states (such as solid surface concentration and electrolyte concentration) that cannot be obtained in the equivalent circuit model[16]. Vilsen et al. reduce the amount of data that needs to be transmitted by extracting descriptive characteristics of the voltage, thereby reducing the number of characteristics. The extracted features are reduced in two stages. The above studies need to identify the internal parameters of Li-ion battery. Once the impedance parameters of Li-ion battery are obtained, it is difficult to avoid the damage experiment on the battery, and the prediction time is long, which easily leads to the delay of information acquisition [17]. The second type is ampere hour method [18]. Ampere hour method can quickly calculate the current change of Li-ion battery, but ampere hour method belongs to open-loop inspection in control. If the current acquisition accuracy is not high, the given initial State of Charge (SOC) [19-22] has a certain error. As the system runs longer, the initial errors will gradually accumulate. The third type is the cyclic method . The principle of the cyclic method is simple and does not need process measurement of various parameters [23, 24], but it requires high accuracy of cycle number statistics. Although the advantages and disadvantages of the cyclic method are very prominent, there are not many researchers to make up for its shortcomings.

At present, the research on battery health mainly focuses on impedance measurement and capacity tests . In contrast, there are few studies on the cycle life of Li-ion batteries. Besides, due to the strong nonlinear [25-28] characteristics of Li-ion batteries, there is little in-depth discussion on the effective cycle criteria of Li-ion batteries, and most studies use the criteria based on impedance and capacity [29-32]. As a result, the shortcomings of the cyclic method that it is difficult to accurately estimate the number of cycles has not been compensated.

In this study, a new method based on the traditional cycle method is proposed to predict the cycle life of Li-ion batteries, and a new idea is provided for the life estimation of Li-ion batteries. This study uses unscented Kalman filter (UKF) algorithm to estimate SOC to solve the problem that ampere hour method is easy to be affected by noise, and provide accurate preliminary data for accurate prediction of SOH. Secondly, because of the strong nonlinearity of Li-ion batteries, it is very difficult to calculate the number of cycles. Therefore, this paper puts forward the idea of integrating small cycles and retaining large cycles, and improves Rainflow algorithm to reduce the sensitivity to data peaks, which is successfully applied to the field of batteries. Based on the improved Rainflow algorithm to accurately calculate the cycle times of SOC, a linearization criterion is proposed to linearize the life prediction of

Li-ion batteries. The results show that this method can predict the remaining life of Li-ion battery with low error without measuring process parameters.

2. MATHEMATICAL ANALYSIS

2.1. Model building

Thevenin model contains a voltage source and an RC parallel circuit. The circuit composed of equivalent polarization internal resistance and equivalent polarization capacitance is used to make up for the shortcoming that the internal resistance model can not describe the dynamic characteristics of Li-ion battery, and the model is easy to implement, as shown in Fig. 1.

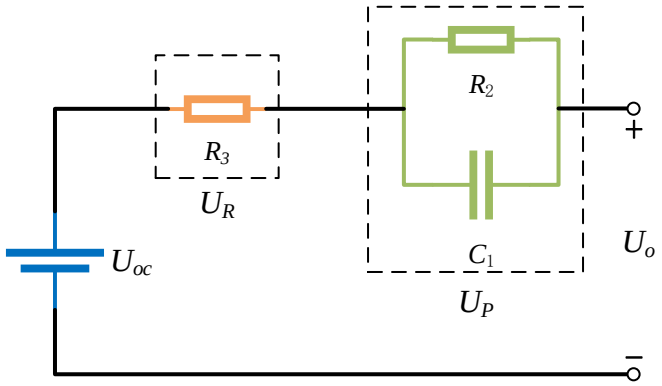

Figure 1. First-order RC circuit model

In Fig.1, U_{OC} is the terminal voltage of the power supply, U_O is the open-circuit voltage, R_1 is the ohmic resistance, U_R is the ohmic voltage, and the polarization voltage of RC parallel circuit composed of polarization resistance R_2 and polarization capacitance C_1 is up. According to the actual demand, combined with Thevenin equivalent circuit model, only SOC is selected as the system state variable, and the battery terminal voltage U_{OC} is taken as the observation variable of the system. The battery state-space expression established is shown in Eq. (1).

$$\begin{cases} SOC_{k+1} = SOC_k - I_k \, \Delta t / Q_N + \omega_k \\ U_{0,k+1} = f(SOC_{k+1}) - U_R - U_1 + \upsilon_{k+1} \end{cases} \quad (1)$$

In Eq. (1), Δt is the sampling interval time, Q_N is the rated capacity of the battery. The actual capacity calibration is required. I_k is the current of time k, and the charging direction is positive. The SOC value of time k+1 is predicted by time k. $U_{o,\,k+1} = f(SOC_{k+1})$ is the experimental method to determine the relationship between the open-circuit voltage of the battery and the SOC of Li-ion batteries. ω_k and v_{k+1} are process noise and observed noise respectively.

2.1. Adaptive Unscented Kalman Filtering

Kalman filter is the state equation and the observation equation of linear system. By observing the input and output of the system, the optimal estimation of the minimum variance of the state is carried out. The implementation of UKF can be divided into forecast stage and update stage.

In the prediction stage, the predicted values of system state variables at time $k + 1$ are shown in Eq. (2).

$$\begin{cases} x^i_{k+1/k} = f(x^i_k, u_k) \\ \hat{x}_{k+1/k} = \sum_{i=0}^{2n} \omega^i_m x^i_{k+1/k} \end{cases} \tag{2}$$

x^i_k is the sampling point using traceless transformation, where $i = 1,2,3\ldots2n + 1$, U_k is the input variables. Combined with the first part of Eq. (2), the sampling points are further predicted. After weighted sum, the predicted mean value of system state variables is obtained, as shown in the second part of Eq. (2). The error variance matrix at $k + 1$ time is also predicted as shown in the fourth part of Eq. (3).

$$\begin{cases} x^i = \hat{x}, i = 0 \\ x^i = \hat{x} + (\sqrt{(n+\lambda)P})_i, i = 1 \sim n \\ x^i = \hat{x} - (\sqrt{(n+\lambda)P})_{i-n}, i = n+1 \sim 2n \\ P_{x,k+1/k} = \sum_{i=0}^{2n} \omega^i_c \left[x^i_{k+1/k} - \hat{x}_{k+1/k} \right] \left[x^i_{k+1/k} - \hat{x}_{k+1/k} \right]^T + Q_k \end{cases} \tag{3}$$

Sigma sample points are updated by the second part of Eq. (2) and combined Eq. (3). The further prediction value of each sampling point at $k + 1$ time is introduced into the observation equation of the system, and the observation prediction value of each sampling point at $k + 1$ time is obtained, and then the average value of measurement value at $k + 1$ time is weighted, as shown in Eq. (4).

$$\begin{cases} y^i_{k+1/k} = h(x^i_{k+1/k}, u_{k+1}) \\ \hat{y}_{k+1/k} = \sum_{i=0}^{2n} \omega^i_m y^i_{k+1/k} \end{cases} \tag{4}$$

$P_{yy,\,k+1}$ is the variance matrix of the measured value at the time of $k + 1$, $P_{xy,\,k+1}$ are the state variables at the time of $k + 1$. R_{k+1} is the expected value of observation noise at k+1 time. And the measured covariance is shown in Eq. (5).

$$\begin{cases} P_{yy,k+1} = \sum_{i=0}^{2n} \omega^i_c \left[y^i_{k+1/k} - \hat{y}_{k+1/k} \right] \left[y^i_{k+1/k} - \hat{y}_{k+1/k} \right]^T + R_{k+1} \\ P_{xy,k+1} = \sum_{i=0}^{2n} \omega^i_c \left[x^i_{k+1/k} - \hat{x}_{k+1/k} \right] \left[y^i_{k+1/k} - \hat{y}_{k+1/k} \right]^T \end{cases} \tag{5}$$

In the update stage, the measured value is compared with the calculated value to make the result more accurate. The calculated Kalman filter gain is shown in the first part of Eq. (6). $\hat{x}_{k+1/k+1}$ is the value of the updated system state variable, as shown in the second part of Eq. (6). $P_{x,k+1/k+1}$ is the update of the error variance matrix, as shown in the third part of Eq. (6).

$$\begin{cases} K_{k+1} = P_{xy,k+1} / P_{yy,k+1} \\ \hat{x}_{k+1/k+1} = \hat{x}_{k+1/k} + K_{k+1}(y_{k+1} - \hat{y}_{k+1/k}) \\ P_{x,k+1/k+1} = P_{x,k+1/k+1} = P_{x,k+1/k} - K_{k+1} P_{xy,k+1} K_{k+1}^T \end{cases} \quad (6)$$

When using UKF to estimate the SOC value of Li-ion battery, SOC and up are generally selected as state variables. After the initialization of state variables, the algorithm predicts and updates the SOC of the battery in each sampling period. At the same time, according to the error covariance, the Kalman gain will be adjusted continuously, and the estimation error will be corrected by feedback.

2.2. Improved Rainflow algorithm

The Rainflow algorithm, also known as the tower top algorithm, was proposed by two British engineers M. Matsuishi and T. Endo in the 1950s. The main function of this counting method is to simplify the actual measured load history into several load cycles, and each cycle is a damage accumulation. This method is widely used in fatigue life calculation, and its main manifestation is load-time curve. At the same time, to reduce the number of half-cycles, it is necessary to reconstruct the time history of the data before counting and move the absolute value of the peak or trough to the starting point of the process, as shown in Fig. 1. In the estimation of Li-ion battery life, the load is SOC, both a set of SOC-time curves are obtained, and then the entire coordinate system is rotated 90 degrees clockwise, and the time coordinate axis is vertically downward. The roof goes down as shown in Fig. 2.

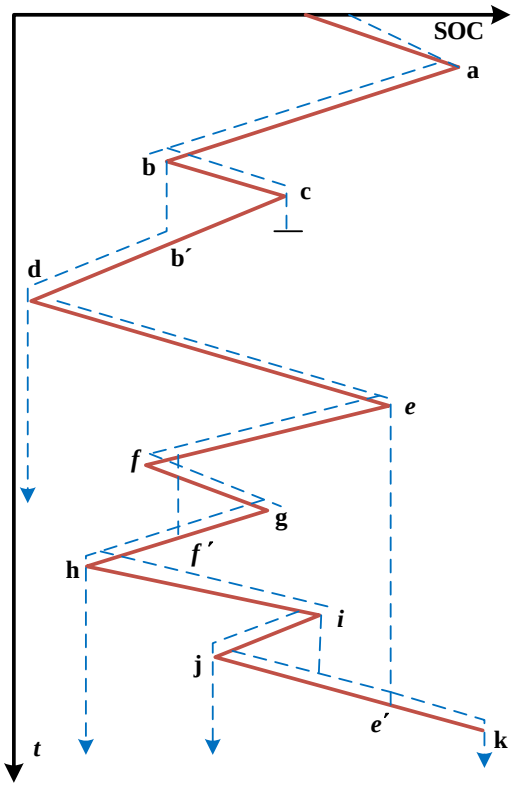

Figure 2. The time history of SOC

The counting rules are as follows:

(1) The Rainflow algorithm starts from the internal measurement of the peak position of the load time history and flows down the slope.

(2) The rain current starts to flow from a certain peak point, and stops flowing when it encounters a larger peak than its actual peak.

(3) When the rain current meets the rain flowing down, it must stop flowing.

(4) Take out all the full cycles and note the amplitude of each cycle.

(5) The divergent convergent load time history remaining after counting in the first stage is equivalent to a convergent divergent load time history, and the second stage rain flow counting is performed. The total number of counting cycles is equal to the sum of the counting cycles of the two counting stages.

According to the above counting process and rules, the SOC time record shown in Fig. 2 includes three complete cycles *b-c-b′, f-g-f″, i-j-e′* and three half cycles *a-b-d, d-e-e′, e-f-h*.

The flow chart of improved Rainflow algorithm is shown in Fig. 3.

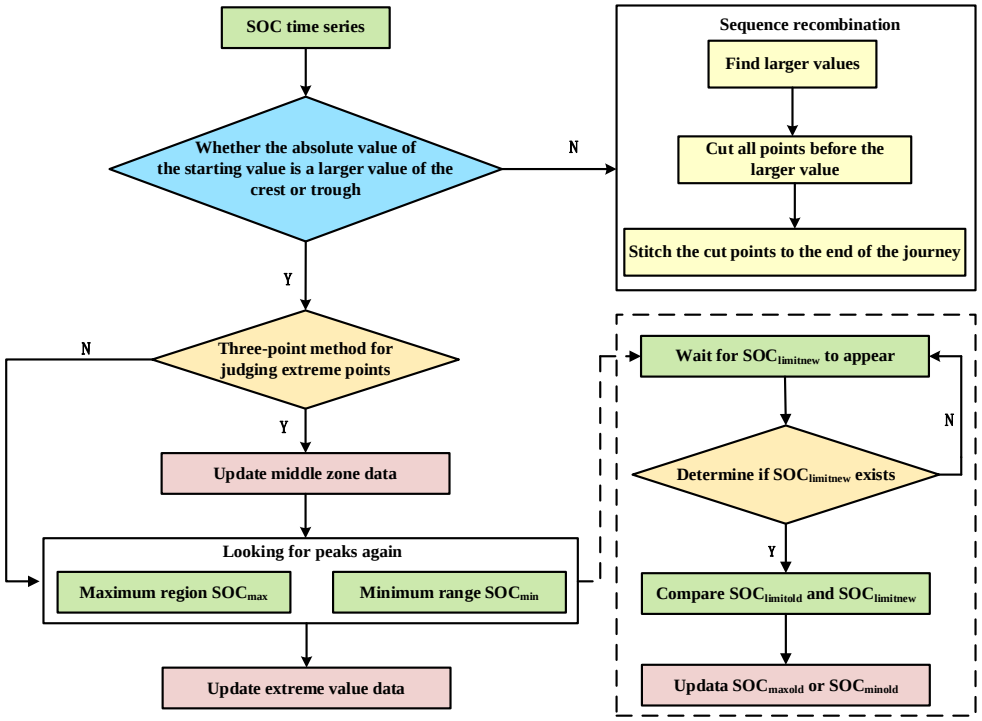

Figure 3. Improvement of Rainflow process

First judge whether the starting value is the peak value. If not, the data before the peak value is cut to the end of the data segment, and the peak value is taken as the starting value. The maximum and minimum values are determined by three-point method, and the data are updated at any time. The middle zone is used to store extreme points. According to the counting principle of the Rainflow algorithm mentioned above, Li-ion batteries may experience some small cycles during a deep cycle. These small cycles may be a small range of charge and discharge, or they may be the oscillation caused by the

electrochemical properties of Li-ion batteries. Due to the advantages of Li-ion batteries, the impact of these small cycles on the life of Li-ion batteries can be ignored. Besides, the traditional Rainflow algorithm is sensitive to the size of the cycle. Therefore, the small cycles in these processes can be filtered out by the improved Rainflow algorithm.

The traditional Rainflow algorithm estimates the load level by calculating the average stress. This method can also be used as a reference for Li-ion batteries load level, but the traditional calculation formula is not suitable for Li-ion batteries load calculation. Formula modification is shown in Eq. (17).

$$D_m = \frac{1 - DOD_{\min} + DOD_{\max}}{2} \tag{17}$$

$DOD_{\max}$ and $DOD_{\min}$ in Eq. (17) are the maximum and minimum Discharge Depths (DOD) of a group of charge-discharge cycles. SOC is obtained by UKF first, and then the data is obtained by counting the Rainflow of SOC. The calculated results are in the range of 0-100. The larger the calculated value is, the heavier load of Li-ion batteries is, and vice versa. Therefore, the average DOD of D_m is used to evaluate the battery load.

3. EXPERIMENTAL ANALYSIS

3.1. Simulation platform building

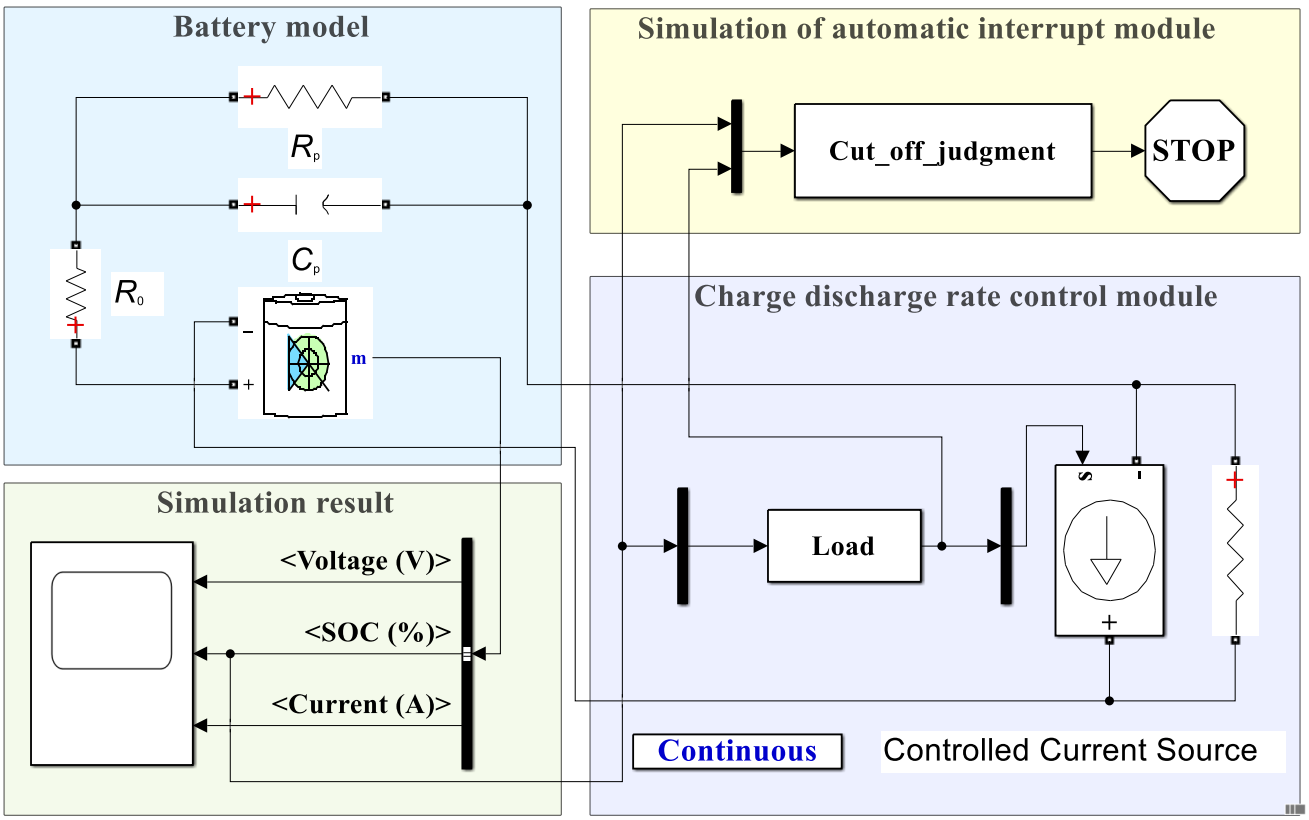

Figure 4. Simulation of Li-ion battery cycle test

In this paper, Li-ion battery module is used to simulate the aging process of battery. The module can set and adjust the aging parameters. The built-in function of load module can adjust the load value of controlled current source according to the SOC of Li-ion battery, and then control the charge and discharge of Li-ion battery.

In Fig. 4, the internal resistance R_0, polarization resistance R_P and polarization capacitance C_P of Li-ion battery are all identified by real Li-ion battery parameters. The charge and discharge current of Li-ion battery is controlled by a controlled current source. The load module controls the DOD. The Li-ion battery is set to 4.2V/70Ah. Relying on the experimental platform in Figure 4, the 1C discharge rate is used under 20% DOD, 50% DOD, 60% DOD, 80% DOD and 95% DOD, and the cyclic DST conditions are used for cyclic experiments.

3.2. Constant current discharge experiment analysing

The parameters of Li-ion battery are set at 4.2V/70Ah and the cut-off voltage is 2.75V. Discharge to 40% and 20% respectively at 1C rate, and then fully charge at 1C rate. Based on the equivalent circuit model, UKF is used to fit and track the SOC of Li-ion battery. The tracking effect is shown in Fig. 5.

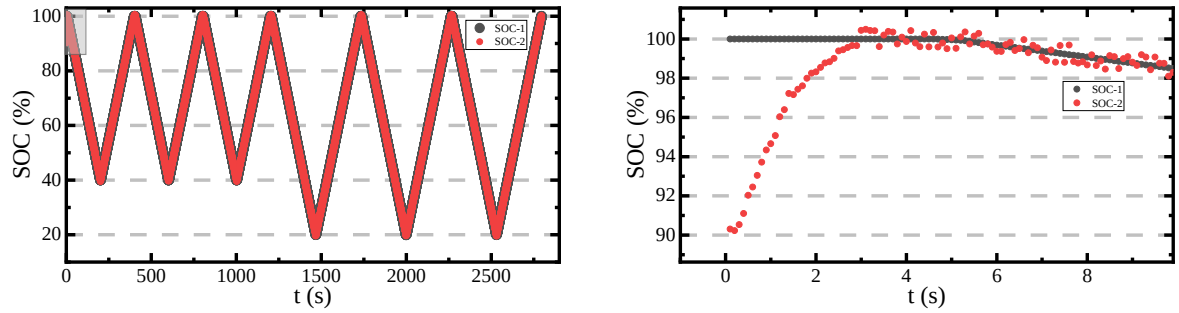

(a) Tracking effect of UKF at 40% and 20% SOC calibration (b) Partial enlargement of SOC initial value

Figure 5. UKF-SOC Estimation under constant current discharge and charge

Fig. 5 shows a comparison of UKF estimates with actual values. SOC-1 is the actual value and SOC-2 is the estimated value. The initial SOC of Li-ion battery is 100%, while the initial value of UKF is set to 90%. As can be seen from Fig.5, UKF quickly tracks the real value, and has excellent robustness. The overall error is controlled within 1%, which fully meets the accuracy requirements of this experiment.

3.3. DOD and Rainflow algorithm Fusion analysing

Rainfall can identify events similar to constant amplitude load data in complex load sequences. Fig. 6 (a) shows that the Li-ion battery completes 700 cycles at 80% DOD, which is called the first load. Fig. 6 (b) shows that the Li-ion battery completes 70 cycles at a DOD of 95%, which is called the second

load. Fig. 6 shows the continuous cycling of the same battery under two different loads. The calculation times of the algorithm are consistent with the actual number of cycles, which proves that the algorithm has good robustness.

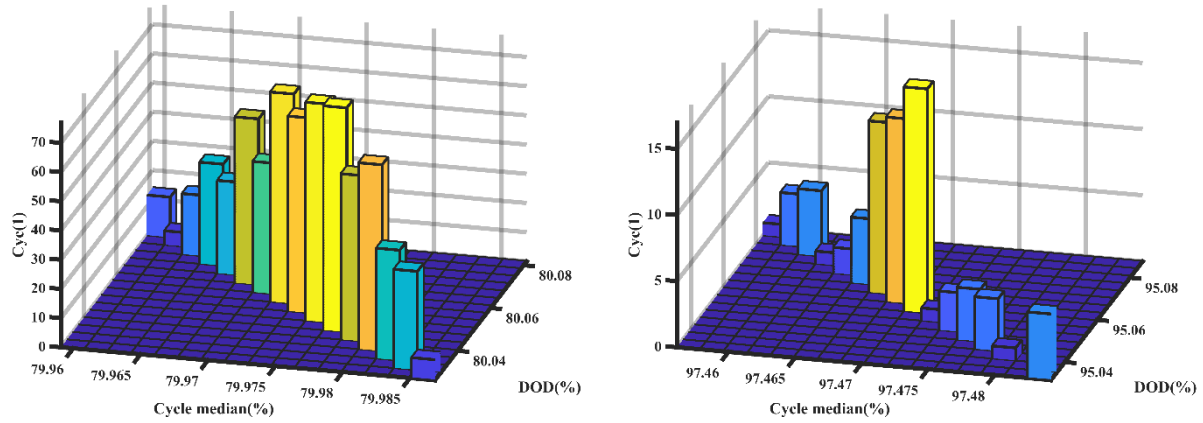

(a) SOC cycle count of 80% DOD (b) SOC cycle count of 95% DOD

Figure 6. Number of battery cycles at different DOD

The Cycle median value in Fig. 6 represents the average stress, and the calculation formula is shown in Equation 17. The end of life of a lithium-ion battery is defined as the damage when the current full capacitance drops to 80% of the initial capacity. However, when the battery capacity is less than 80%, it can still be used, but the performance of the lithium-ion battery will decrease. The meaning of average stress here is that when the damage of the lithium-ion battery exceeds the specified value, the stress level should be reduced during use. Avoid further deep discharge of the battery, that is, reduce the battery load. DOD shows the corresponding DOD of lithium-ion batteries under different average stresses. Cyc shows the number of cycles of the battery at different cycle depths. The median cycle value in Figure 6(a) is lower than that in Figure 6(b), indicating that the damage of the battery under 95% DOD is more serious than under 80% DOD.

3.4. Linear damage criterion

3.4.1. Criteria constructing

Due to the chemical characteristics of Li-ion battery, its properties show strong nonlinearity in use. Therefore, it is difficult to estimate the remaining life of Li-ion battery. The linear damage model proposed in this paper can quickly estimate battery life.

No matter in the condition of regular or irregular changes in current, as long as the battery completes a charge-discharge cycle, it will accumulate the next damage, and multiple damage accumulation will eventually lead to battery failure. All cycles of the battery under the first condition are called the first load N_1, and all cycles under the second condition are called the second load N_2. And so on, until the N_i load, the battery fails. Then, the total number of cycles N_f of the battery at fatigue failure given by the manufacturer is introduced. If the damage curve with the number of cycles of $N_{i,f}$ as the

abscissa is linearized, the linear damage criterion can be derived by simplifying the damage curve to a single line with the cycle ratio of $N_i / N_{i,f}$ as the abscissa. In this case, no matter how the current changes, there is a unique linear relationship between fatigue damage and cycle ratio. Therefore, when the damage level is given, the cycle ratio of different damage curves will be the same, as shown in the Fig. 7.

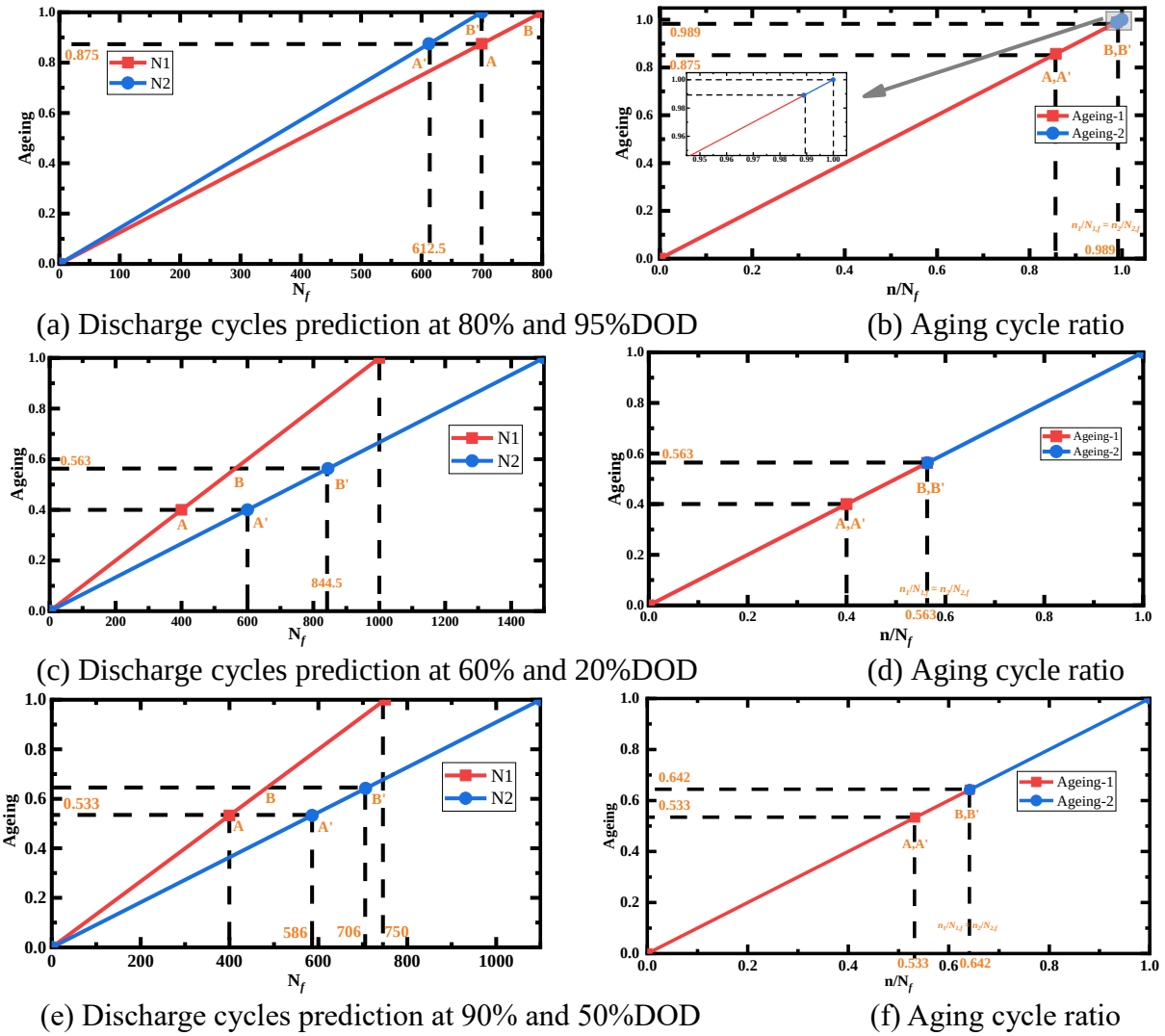

(a) Discharge cycles prediction at 80% and 95%DOD (b) Aging cycle ratio

(c) Discharge cycles prediction at 60% and 20%DOD (d) Aging cycle ratio

(e) Discharge cycles prediction at 90% and 50%DOD (f) Aging cycle ratio

Figure 7. Linear aging accumulation under different conditions

In Fig. 7, all the working conditions are linear prediction graphs based on the number of cycles counted by Rainflow algorithm. In Fig. 7 (a), N_1 is the cyclic load case of Li-ion battery at 80% discharge depth, i.e. the first load. In the case of the first load, the total life of the Li-ion battery is 800 times, and the actual number of cycles is 700. At this time, it can be seen from the figure that the aging calculation value of the battery is 0.875. N_2 is the second load of Li-ion battery at 95% discharge depth. Since the DOD of N_2 is deeper than that of N_1, the lifetime of Li-ion battery under this condition is 700 times. The second load is superimposed on the first load, so look for point B on N_2 which is the same as N_1 aging. The curve section after point B' is the aging superposition section. The cycle ratio is divided by the

number of cycles under load and the total number of theoretical cycles under the load. The next load case is treated in the same way, and finally spliced with this method. The result is shown in Fig. 7 (b). In Fig. 7 (b), Aging-1 is the aging that has occurred, and Aging-2 is the prediction of Li-ion battery aging after the end of N_2 based on N_2 load. In this way, no matter what the DOD, there is a unique linear relationship between the Li-ion battery Aging and the cycle ratio. When the aging accumulated to 1, the Li-ion battery fatigue failed. Similarly, Fig. 7 (c) and Fig. 7 (d) show the aging prediction chart with 60% DOD discharge and then 20% DOD discharge. Fig. 7 (e) and Fig. 7 (f) show the aging prediction chart with 90% DOD and then 50% DOD. This prediction method avoids the tedious parameter identification in reference [16].

3.4.2. Criteria validating

According to the experimental data of battery cycle life under different working conditions, the SOH curve was drawn. Fig. 8 shows the curves of battery SOH under different DOD.

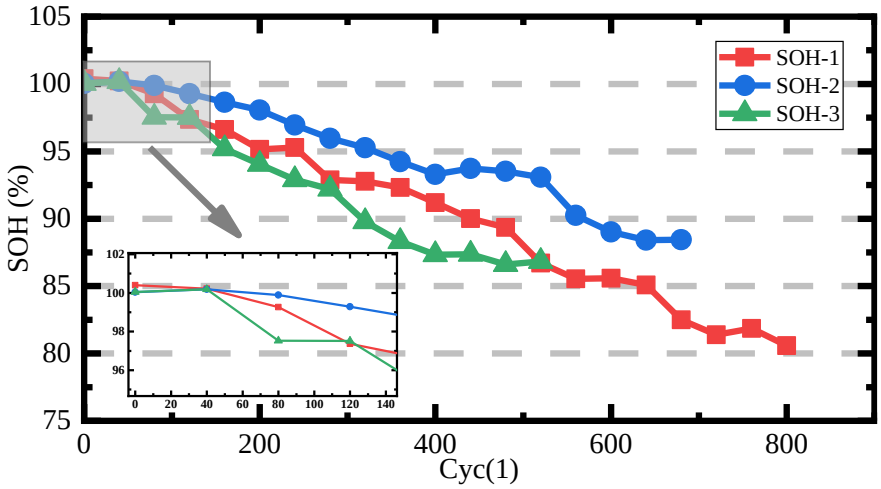

Figure 8. Variation curve of SOH under different DOD values

In Fig. 8, SOH-1 shows the change curve of SOH when the Li-ion battery is charged and discharged with 80% DOD 700 times and then charged and discharged with 95% DOD 80 times. SOH-2 is the change curve of SOH when the Li-ion battery is charged and discharged with 60% DOD 400 times and then charged and discharged with 20% DOD 280 times. SOH-3 is the change curve of SOH when the Li-ion battery is charged and discharged with 90% DOD 400 times and then charged and discharged with 50% DOD 120 times.

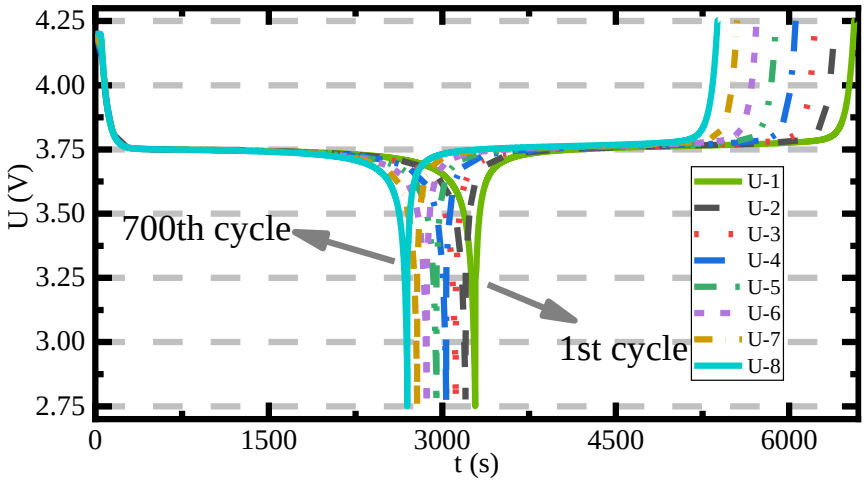

Figure 9. The curve of voltage changing with increasing cycle times under 100% DOD

Fig. 9 shows the voltage change curve of a Li-ion battery at 100% DOD. U1-U8 are the voltage data recorded every 100 cycles. It can be seen from the figure that as the number of cycles increases, the discharge time of the Li-ion battery under the same DOD is shortening, that is, the time for the Li-ion battery voltage to drop from 4.2V to the cut-off voltage 2.75V is gradually shortening. This is in line with the real aging of Li-ion batteries, which proves that the Li-ion battery simulation model in this article is reliable, which provides reliable data support for the linear prediction method proposed in this article.

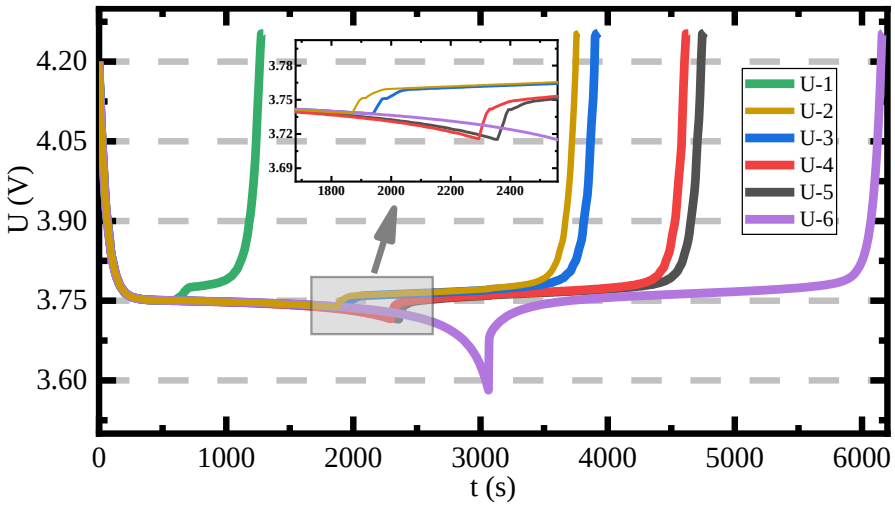

Figure 10. Voltage change curve under different DOD

U1-U6 in Fig. 10 shows the charging and discharging voltage curves of Li-ion battery at 280 cycles of 20% DOD, 120 cycles of 50% DOD, 400 cycles of 60% DOD, 700 cycles of 80% DOD, 400 cycles of 90% DOD and 80 cycles of 95% DOD. It can be seen that the working voltage of Li-ion battery

is maintained at about 3.75V. The deeper the discharge, the lower the voltage. When the voltage is lower than the working voltage, the battery aging will be aggravated. This also proves that the battery load estimate D_m proposed in Eq. 17 is reliable.

Based on all the above data, the comparison results between the real value of Li-ion battery aging and the value obtained by the aging linear prediction method proposed in this paper are shown in Table 1.

Table 1. Comparison between simulation and prediction damage

	SOH-1	SOH-2	SOH-3
Load 1 (DOD)	80%	60%	90%
Cycle times	700	400	400
Load 2 (DOD)	95%	20%	50%
Cycle times	80	280	120
Predicting damage	0.989	0.586	0.642
Actual damage	1	0.578	0.659
Error	1.10%	1.36%	2.53%

It can be seen from Table 1 that each SOH prediction is based on the superposition of two different DOD conditions at 25℃. Under the three conditions, the maximum error is 2.53%, and this prediction method avoids the tedious parameter identification in reference [16]. Compared with literature [15] (the maximum short-term prediction error of SOH is 4%) and [33] (the maximum prediction error is 5%), the prediction method proposed in this paper reduces the maximum prediction error by 1%-2.5% . Therefore, the linear prediction model based on the improved Rainflow algorithm can achieve the purpose of predicting Li-ion battery damage.

4. CONCLUSIONS

Based on the theoretical basis of the cyclic method, this research proposes a new method for predicting the life of Li-ion batteries, and also provides a new solution for the field of Li-ion battery cycle inspection. Due to the nonlinearity of Li-ion battery, many small cycles will be introduced in the cycle process, and the impact of these small cycles on life can be ignored. Based on this, an improved Rainflow algorithm is proposed, which can be applied in the field of Li-ion batteries by adding the intermediate judgment area and changing its definition. After hundreds of cycles with different discharge depths, the improved rain flow counting method can still accurately count the number of cycles, which has solved the application problem of Rainflow algorithm in Li-ion battery field and eliminates the error of traditional Rainflow algorithm. Moreover, this method can skip the steps of impedance and capacity tests, which is very convenient and simple. Finally, to achieve the purpose of prediction, a linear damage criterion is proposed to linearize the life prediction of Li-ion batteries. The errors of three groups of

working conditions are 1.1%, 1.36%, 2. 53%. It has the characteristics of high precision. Because this study does not need to introduce special equipment, and all data can be obtained in real time. Therefore, this method can be introduced into BMS, and can be applied to electric vehicles, UAVs, energy storage equipment and other fields to improve the security and prediction efficiency of power supply.

ACKNOWLEDGEMENTS
The work was supported by National Natural Science Foundation of China (No. 61801407), Sichuan s cience and technology program (No. 2019YFG0427), China Scholarship Council (No. 201908515099) and Fund of Robot Technology Used for Special Environment Key Laboratory of Sichuan Province (No. 18kftk03).

References

1. M. S. Kim, M. S. Kim, V. Do, Y. Xia, W. Kim and W. I. Cho, *J Power Sources*, 422 (2019) 104.
2. C. X. Xie, Y. Liu, W. J. Lu, H. M. Zhang and X. F. Li, *Energ Environ Sc.i*, 12 (2019) 1834.
3. Q. Zhao, J. X. Zheng and L. Archer, *Acs Energy Lett*, 3 (2018) 2104.
4. J. G. Han, J. B. Lee, A. Cha, T. K. Lee, W. Cho, S. Chae, S. J. Kang, S. K. Kwak, J. Cho, S. Y. Hong and N. S. Choi, *Energ Environ Sci.*, 11 (2018) 1552.
5. M. Bayati, M. Abedi, M. Farahmandrad and G. B. Gharehpetian, *Ieee T Power Electr.*, 36 (2021) 1295.
6. M. Astaneh, R. Dufo-Lopez, R. Roshandel and J. L. Bernal-Agustin, *Int J Elec Power*, 103 (2018) 115.
7. B. Kumar, N. Khare and P. K. Chaturvedi, *Microelectron Reliab*, 84 (2018) 66.
8. G. S. d. Santos, F. J. Grandinetti, R. A. R. Alves and W. d. Q. Lamas, *IEEE Latin America Transactions*, 18 (2020) 1345.
9. D. Li, Z. S. Zhang, P. Liu, Z. P. Wang and L. Zhang, *Ieee T Power Electr.*, 36 (2021) 1303.
10. R. H. Jiao, K. X. Peng and J. Dong, *Ieee T Instrum Meas.*, 69 (2020) 8831.
11. H. B. Ren, Y. Z. Zhao, S. Z. Chen and T. P. Wang, *Energy*, 166 (2019) 908.
12. D. Yang, X. Zhang, R. Pan, Y. J. Wang and Z. H. Chen, *J Power Sources*, 384 (2018) 387.
13. J. Li, K. Adewuyi, N. Lotfi, R. G. Landers and J. Park, *Appl Energy*, 212 (2018) 1178.
14. H. Ji, W. Zhang, X. H. Pan, M. Hua, Y. H. Chung, C. M. Shu and L. J. Zhang, *Int J Energ Res.*, 44 (2020) 6502.
15. G. Z. Dong, Z. H. Chen, J. W. Wei and Q. Ling, *Ieee T Ind Electron*, 65 (2018) 8646.
16. X. S. Hu, D. P. Cao and B. Egardt, *Ieee-Asme T Mech.*, 23 (2018) 167.
17. F. Q. Chang, F. Roemer and M. Lienkamp, *Ieee T Power Electr.*, 35 (2020) 11879.
18. X. Xiong, S. L. Wang, C. Fernandez, C. M. Yu, C. Y. Zou and C. Jiang, *Int J Energ Res.*, 44 (2020) 11385.
19. X. J. Tan, Y. Q. Tan, D. Zhan, Z. Yu, Y. Q. Fan, J. Z. Qiu and J. Li, *Ieee Access*, 8 (2020) 56811.
20. J. H. Meng, M. Ricco, G. Z. Luo, M. Swierczynski, D. I. Stroe, A. I. Stroe and R. Teodorescu, *Ieee T Ind Appl.*, 54 (2018) 1583.
21. X. Lai, Y. J. Zheng and T. Sun, *Electrochim Acta*, 259 (2018) 566.
22. L. Cai, J. H. Meng, D. I. Stroe, J. C. Peng, G. Z. Luo and R. Teodorescu, *Ieee T Power Electr.*, 35 (2020) 11855.
23. M. Baumann, L. Wildfeuer, S. Rohr and M. Lienkamp, *J Energy Storage*, 18 (2018) 295.
24. Z. B. Wei, C. F. Zou, F. Leng, B. H. Soong and K. J. Tseng, *Ieee T Ind Electron.*, 65 (2018) 1336.
25. C. F. Zou, X. S. Hu, S. Dey, L. Zhang and X. L. Tang, *Ieee T Ind Electron.*, 65 (2018) 5951.
26. R. Bermejo and R. G. del Sastre, *Appl Math Comput.*, 361 (2019) 398.

27. N. Harting, N. Wolff, F. Roder and U. Krewer, *J Electrochem Soc.*, 166 (2019) A277.
28. M. D. Murbach, V. W. Hu and D. T. Schwartz, *J Electrochem Soc.*, 165 (2018) A2758.
29. Y. Li, M. Abdel-Monema, R. Gopalakrishnan, M. Berecibar, E. Nanini-Maury, N. Omar, P. van den Bossche and J. Van Mierlo, *J Power Sources*, 393 (2018) 230.
30. S. Gantenbein, M. Schonleber, M. Weiss and E. Ivers-Tiffee, *Sustainability-Basel*, 11 (2019).
31. X. Liang, J. F. Yun, Y. Wang, H. F. Xiang, Y. Sun, Y. Z. Feng and Y. L. Yu, *Nanoscale*, 11 (2019) 19140.
32. Y. J. Zheng, J. J. Wang, C. Qin, L. G. Lu, X. B. Han and M. G. Ouyang, *Energy*, 185 (2019) 361.
33. S. B. Vilsen and D. I. Stroe, *J Clean Prod.*, 290 (2021)